SUPPORTING INFORMATION

INCREASED LI-ION PORE ACCESS THROUGH DEVELOPMENT OF LITHIUM ETHYLENE DICARBONATE SEI BY PASSIVATION OF OXIDIZED AMORPHOUS CARBON ELECTRODE WITH FLUOROSURFACTANT

John Collins, Dong Zheng, Tue Ngo, Deyang Qu, Michelle Foster*

Supplemental Figure 1 displays the C-F and C-O-C / C-O-H stretching peak identities and intensities for the fluorosurfactant used in the present study. Concentrations displayed span across the range of those applied to the oxidized carbon used in the present study. C-O stretching frequencies of SOGs arise in the 1000cm^{-1} to 1300cm^{-1} range as determined previously for the E-series, thereby necessitating the method displayed in Figure 1 to eliminate SOG interference from fluorosurfactant intensities. (20)

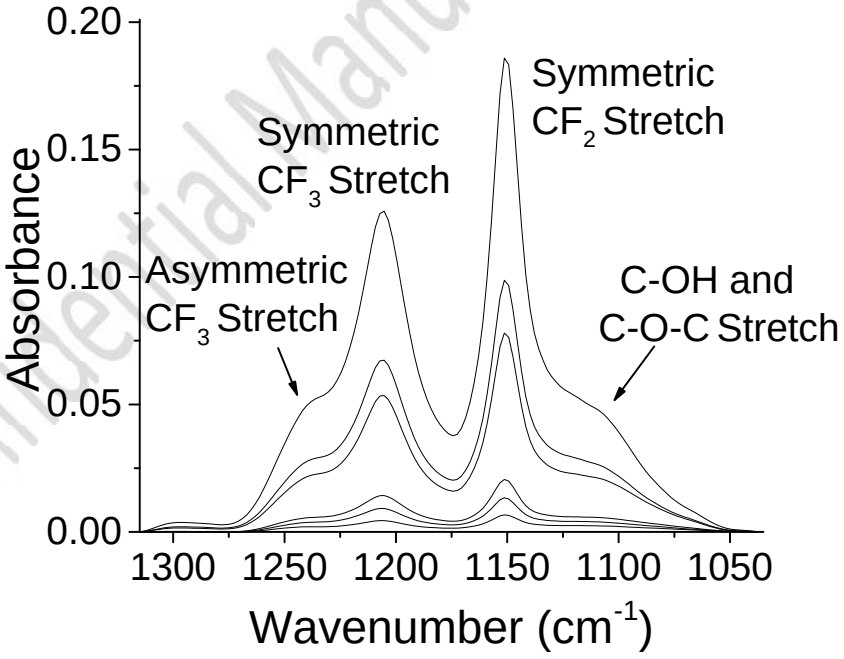

Supplemental Figure 1 Diamond ATR Absorbance of active C-F and C-O-C stretching for FSN Zonyl non-ionic selected concentrations between 0.01% - 0.38% v/v.

Supplemental Figure 2 displays the equilibrium voltage differences between the fully charged and discharged states, for the first 50 cycles of the electrodes used in this study. The more optimized SEI-developed electrodes, E2.075, E2.15 and N2.15, display relatively high equilibrium voltage difference potentials that are sustained through the 50 charge/discharge cycles. Such relatively high equilibrium voltage potentials are attributed to increased Li-ion access to quinone sites. The extensive SEI development displayed for the more optimized surface treated electrodes enables drastic increases in equilibrium voltage differences displayed due to high increases of equilibrium reduction potentials, as quinone sites are accessed in higher concentrations.

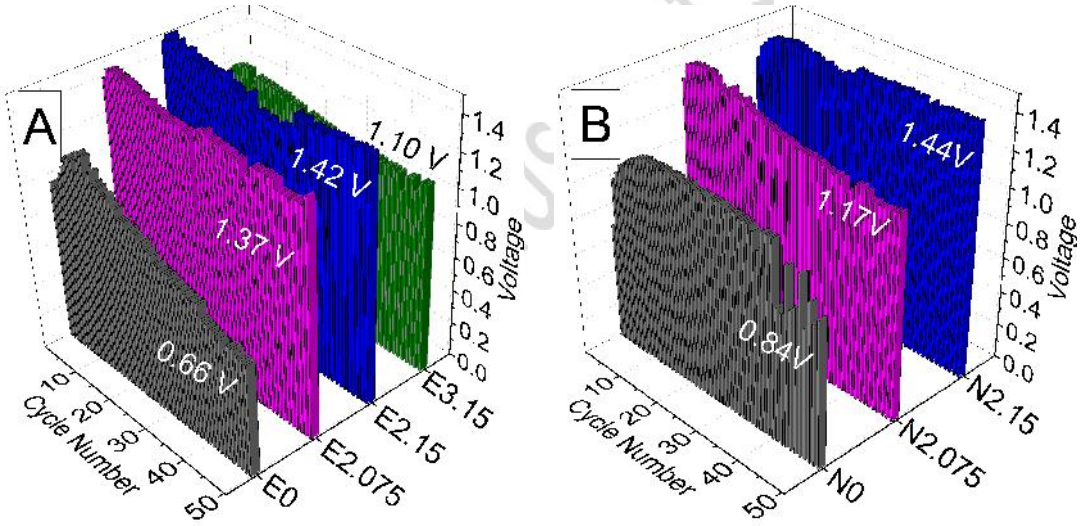

Supplemental Figure 2. Voltage differences for the averaged 50 cycles displayed in **Error! Reference source not found.**. Both charge and discharge equilibrium voltages were obtained after resting the fully charged or discharged carbon electrodes for 2.5 hrs. **(A)** E-series carbon and **(B)** N-series carbon electrodes. Voltages displayed for each plot denote equilibrium working voltage of respective 50th cycle.

Supplemental Figure 3 displays the relative DRIFTS spectra of the N-series electrodes for the mid-IR range investigated. The non-passivated pore structure of the NUC sample remains largely unreactive to electrolyte decomposition at open circuit potential (OCP), and displays a relatively high concentration of solvent on the surface, just as displayed for the EUC electrode in

Figure 8. The N2.075 treated electrode displays similar solvent peak intensities as the NUC electrode, indicating that a high amount of the SOG-coordinated EC solvent was not decomposed. The far majority of the electrochemically accessible surface area for the N0 and N2.15 electrodes facilitates $(CH_2OCO_2Li)_2$ SEI development, as these electrodes display relatively low EC solvent peak intensities combined with high $(CH_2OCO_2Li)_2$ features.

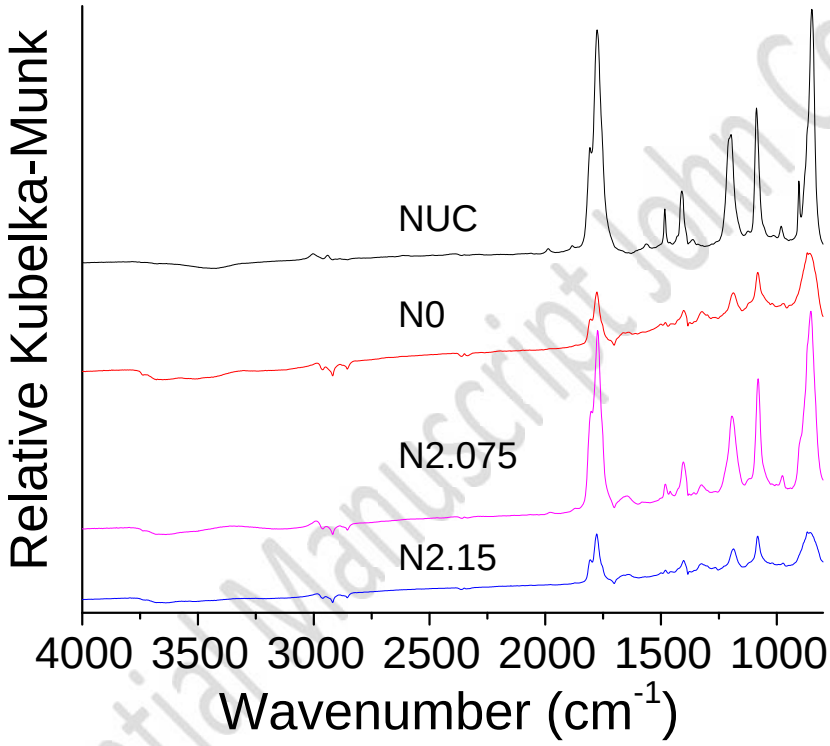

Supplemental Figure 3. Full, raw DRIFTS spectra of N-series carbon electrodes after 50 charge/discharge cycles (at 400uA of applied current (0.1-2.2V) and uncycled carbon electrode (NUC) assembled with identical electrolyte and equilibrated for 48hrs at ~3.0V vs Li. All DRIFT samples were characterized using a 1% carbon:KBr w/w ratio.

Supplemental Figure 4 A displays the baseline corrected EC C=O stretching for the N-series. The N2.075 electrode's coordinated EC peak height is on par with the NUC sample. Similar to the E3.15 electrode, the concentration of surface-solvating EC is quite high—implying a relatively low degree of EC decomposition on active sites. The NUC electrode displays the 3 stretching regions $(CH_2OCO_2Li)_2$, where 1666cm^{-1} and 1640cm^{-1} are the dimer stretching modes

and 1610cm^{-1} is attributed to the trimer stretching mode. The $(CH_2OCO_2Li)_2$ C=O stretching region (Supplemental Figure 4 B_1) for N2.075 displays the highest $(CH_2OCO_2Li)_2$ formation of all the electrodes—with an extensive shoulder protruding < 1620cm^{-1}—indicating significant $(CH_2OCO_2Li)_2$ trimer formation. The N0 and N2.15 samples display similar peak height trends across the board, indicating relatively high solvent decomposition for both electrodes, for each electrode's independently accessible surface area. N0 displays a distinct trimer peak formation (~1610cm^{-1}) whereas N2.15 displays the lowest trimer formation of the treated N-series. Supplemental Figure 4 B_2 displays the $(CH_2OCO_2Li)_2$ bending modes for the N-series. No distinct increase in $(CH_2OCO_2Li)_2$ bending intensity or blue shifting is observed for the N-series electrodes, as was observed for the E-series (Figure 9, B_2).

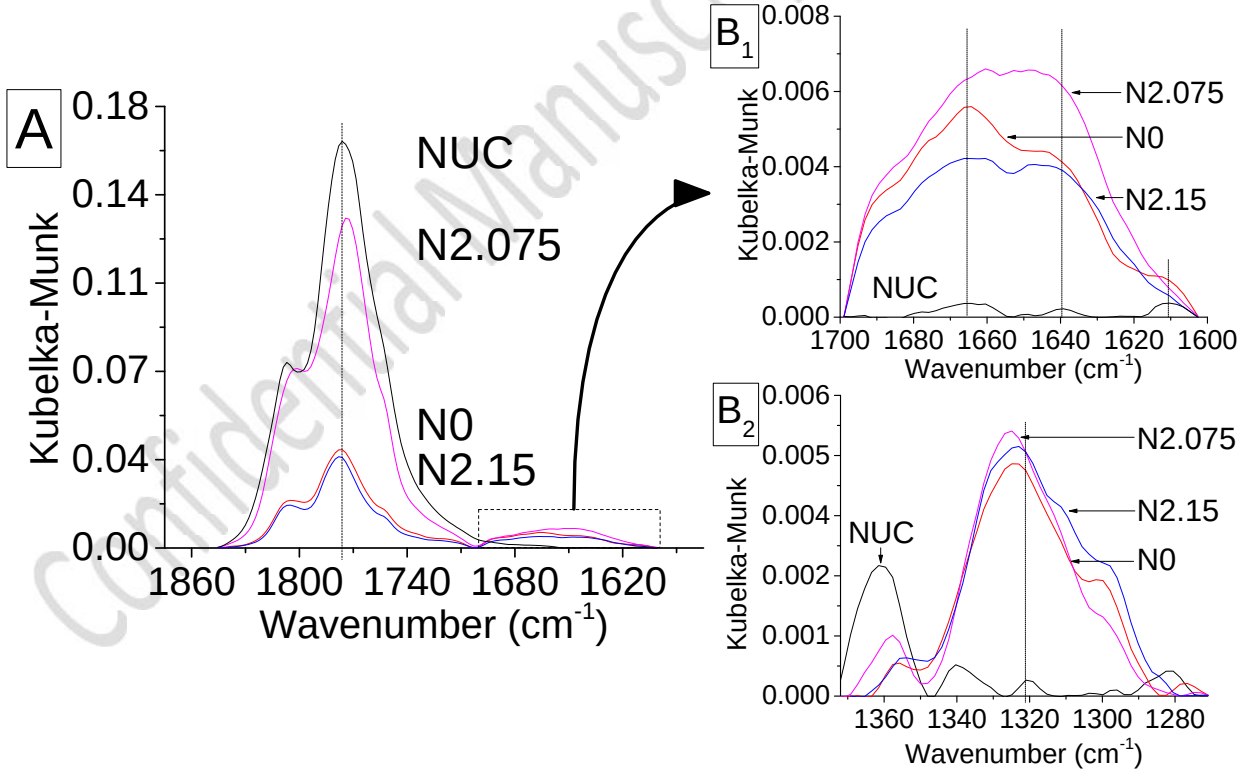

Supplemental Figure 4. N-series Baseline corrected stretching regions for **(A)** EC (C=O st.), **(B_1)** $(CH_2OCO_2Li)_2$ (C=O st.) and **(B_2)** $(CH_2OCO_2Li)_2$ (CH_2 Deformations). Dotted lines indicate peak maximums for respective active mode for NUC sample.